Structural, Kinetic, and Thermodynamic Analysis of Glucoimidazole-Derived Glycosidase Inhibitors[†,‡]

Tracey M. Gloster,[§] Shirley Roberts,[§] Giuseppe Perugino,[∥] Mosè Rossi,[∥] Marco Moracci,[∥] Narendra Panday,[⊥] Miroslav Terinek,[⊥] Andrea Vasella,[⊥] and Gideon J. Davies*[,§]

Structural Biology Laboratory, Department of Chemistry, The University of York, Heslington, York YO10 5YW, United Kingdom, Institute of Protein Biochemistry-CNR, Via P. Castellino 111, 80131 Naples, Italy, and Laboratorium für Organische Chemie, HCI H 317, ETH Zürich, CH-8093 Zürich, Switzerland

Received May 17, 2006; Revised Manuscript Received June 21, 2006

ABSTRACT: Inhibition of glycosidases has great potential in the quest for highly potent and specific drugs to treat diseases such as diabetes, cancer, and viral infections. One of the most effective ways of designing such compounds is by mimicking the transition state. Here we describe the structural, kinetic, and thermodynamic dissection of binding of two glucoimidazole-derived compounds, which are among the most potent glycosidase inhibitors reported to date, with two family 1 β-glycosidases. Provocatively, while inclusion of the phenethyl moiety improves binding by a factor of 20−80-fold, this does not appear to result from better noncovalent interactions with the enzyme; instead, improved affinity may be derived from significantly better entropic contributions to binding displayed by the phenethyl-substituted imidazole compound.

Glycosidase inhibition is of great importance, not only for the insight it provides into enzyme mechanism, but also in the quest for new therapeutic agents in the treatment of cancer, diabetes, lysosomal storage diseases, and viral infections, such as influenza and HIV. Glycosidases provide a rich framework with which to study inhibition through transition state mimicry, due to the extremely tight binding predicted for the transition state. Given the 10^{17}-fold increase in the level of glycosidic bond hydrolysis over that of the uncatalyzed reaction provided by glycosidases, Wolfenden and colleagues propose that glycosidases bind their transition state with a dissociation constant of not greater than 10^{-22} M (*1*). Such tight binding suggests that transition state mimicry should provide extremely potent inhibitors, yet therapeutic agents currently in use, such as Relenza, Tamiflu, and Miglitol, harness only a very small fraction of this transition state binding potential. Furthermore, what actually constitutes a "transition state mimic" and the forces that should govern the binding of such a compound remain open, even controversial, questions (*2*−*4*).

More than 20 000 glycosidase sequences are now known and have been classified into more than 100 glycosidase families based on sequence similarity (see http://afmb.cnrs-mrs.fr/CAZY/) (*5*). This study examines the inhibition of β-glycosidases from *Thermotoga maritima* (*Tm*GH1)[1] and *Sulfolobus solfataricus* (this has historically been abbreviated to *Ss*βGlc1, but here is called *Ss*GH1), which are both placed into family 1 of the CAZy system. *Tm*GH1 and *Ss*GH1 hydrolyze glycosides with overall retention of anomeric configuration using a double-displacement mechanism via a covalent glycosyl−enzyme intermediate. The covalent intermediate is flanked by highly dissociative transition states which possess substantial oxocarbenium ion-like character (Figure 1). Such transition states feature extensive sp^2 hybridization and partial positive charge (predominantly along the bond between the anomeric carbon and endocyclic oxygen) and likely involve pyranoside distortion to half-chair ($^4H_3$ or $^3H_4$ or their closely related envelope form) or boat ($^{2,5}B$ or $B_{2,5}$) conformations (reviewed in ref *6*).

Some of the most powerful glycosidase inhibitors contain imidazole moieties (*7*−*9*), such as the glucoimidazole β-glucosidase inhibitors **1** and **2** (Figure 1), which both display a flattened transition state-mimicking conformation resulting from fusion of the planar imidazole ring to the "glycon". Both compounds also possess a vacant lone pair of electrons for lateral "anti-protonation" by the acid/base residue (*10*, *11*). Compound **2**, which is substituted with a phenethyl group, is proposed to interact with active site residues in the +1 subsite, which would lead to increased potency (*9*). Indeed, such productive interactions between the phenethyl group and aromatic groups in the enzyme were recently observed for compounds **3** and **4** binding to a family GH3 β-D-glucan glucohydrolase (*12*, *13*).

Here we describe the three-dimensional structure, thermodynamic signatures, and inhibition kinetics for compounds

[†] T.M.G. acknowledges the EPSRC for a postgraduate studentship. M.R. and M.M. were supported by MIUR Project RBAU015B47. During the course of this work, G.J.D was a Royal Society University Research Fellow and was supported by the BBSRC.

[‡] PDB files and observed structure factor amplitudes have been deposited as entries 2CES and 2CET for *Tm*GH1 in complex with **1** and **2** and 2CEQ and 2CER for *Ss*GH1 in complex with **1** and **2**, respectively.

* To whom correspondence should be addressed. Telephone: +44 1904 328260. Fax: +44 1904 328266. E-mail: davies@ysbl.york.ac.uk.

[§] The University of York.

[∥] Institute of Protein Biochemistry-CNR.

[⊥] ETH Zürich.

[1] Abbreviations: *Tm*GH1, family 1 β-glucosidase from *Thermotoga maritima*; *Ss*GH1, family 1 β-glycosidase from *Sulfolobus solfataricus*.

10.1021/bi060973x CCC: $33.50
Published on Web 09/12/2006

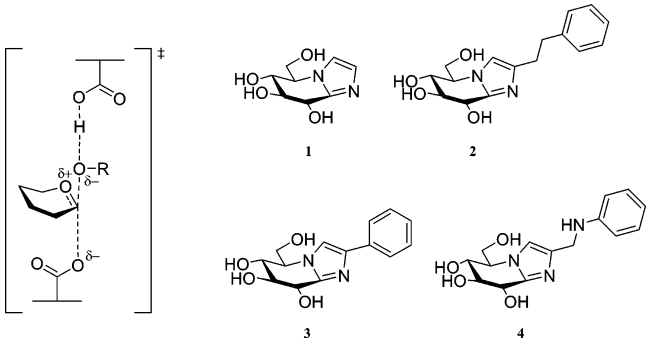

FIGURE 1: Structure of the oxocarbenium ion-like transition state and (**1**) glucoimidazole, (**2**) phenethyl-substituted glucoimidazole, (**3**) phenyl-substituted glucoimidazole, and (**4**) phenylaminomethyl-substituted glucoimidazole.

1 and **2** with the two family 1 β-glucosidases. Surprisingly, while compound **2** binds some 20−80 times stronger than **1**, such affinity does not appear to reflect "better" and more ordered noncovalent interactions between the ligand and the enzyme. Instead, tighter binding is driven by a significantly better entropic contribution to binding of **2**, relative to **1**, despite the observed flexibility of the phenethyl substituent.

EXPERIMENTAL PROCEDURES

X-ray Crystallography. *Tm*GH1 and *Ss*GH1 were expressed, purified, and crystallized as described previously (*2*, *14*). Native *Tm*GH1 crystals were added to a drop of mother liquor containing a minute amount of solid **1** or **2** (synthesis described in ref *7* for **1** and in ref *9* for **2**) and allowed to soak for 5−30 min. Minute amounts of solid **1** or **2** were added to *Ss*GH1 prior to crystallization and allowed to incubate for between 5 min and 2 h. Both *Tm*GH1 and *Ss*GH1 crystals were cryoprotected in a solution containing their respective mother liquor with 25% ethylene glycol and frozen in liquid nitrogen.

Data for all complexes were collected at ESRF (Grenoble, France). Data were processed and scaled with DENZO and SCALEPACK (*15*) (see Table 1 for statistics). All other calculations used the CCP4 suite of programs (*16*). Isomorphism between the native *Tm*GH1 and *Ss*GH1 structures and the complexes meant refinement could commence following rigid body refinement in REFMAC (*17*) (using the protein atoms only from PDB entries 1OD0 and 1GOW, respectively). Small rigid body motions meant that AMoRe (*18*) (resolution range of 15−3 Å, radius of integration of 25 Å) was required to determine the structure of *Ss*GH1 in complex with **2**. Five percent of the observations were set aside for cross validation and were used to monitor refinement strategies (*19*). Manual corrections of the model using COOT (*20*) were interspersed with cycles of least-squares refinement using REFMAC (*17*).

Isothermal Titration Calorimetry. Isothermal titration calorimetry (ITC) was performed using a VC calorimeter (Microcal, Northampton, MA) at 25 °C. *Tm*GH1 was dialyzed into 100 mM sodium citrate buffer (pH 5.8) to a final concentration of 50−60 μM. **1** or **2** was diluted in the same buffer to a final concentration of 0.5 mM. Samples were spun and degassed prior to use. Titrations were performed by injecting 10 μL aliquots of ligand into *Tm*GH1. Data were corrected for the heats of dilution by subtracting the excess heat at a high molar ratio of inhibitor to enzyme. The stoichiometry (n), enthalpy (ΔH), and equilibrium association constant (K_a) were determined from fitting to a bimolecular model using Microcal Origin. The Gibbs free energy (ΔG) and entropy ($T\Delta S$) were calculated using the equations $\Delta G = -RT \ln K_a = \Delta H - T\Delta S$. Sodium citrate buffer was used for the calorimetry experiments to minimize the effect of the buffer heat of ionization; citrate has a ΔH_{ion} that is among the lowest value of all buffers (*21*).

Kinetics. Kinetic studies with *Tm*GH1 and *Ss*GH1 were conducted by monitoring the change in UV−visible absorbance with a Cintra 10 spectrophotometer, equipped with a Thermocell Peltier power supply, at 25 °C. Although *Tm*GH1 and *Ss*GH1 are thermostable proteins, we decided to perform kinetic studies at the same temperature at which ITC was carried out to allow direct comparisons to be made between the different methods and proteins. The dependence of k_{cat}/K_M on pH for *Tm*GH1 was measured using substrate depletion methods at a substrate concentration lower than the K_M, as described in ref *22*. K_i values for **1** and **2** with *Tm*GH1 were determined over the same pH range by monitoring the rates in the absence and presence of inhibitor under steady state conditions, as described in ref *22*; assays contained between 30 nM and 1 μM **1** or between 20 and 50 nM **2**, and *Tm*GH1 concentrations of 1.7−9.1 nM. The enzyme concentration was always at least 10 times lower than the concentration of inhibitor.

K_i values for *Ss*GH1 were also determined under steady state conditions in 25 mM sodium phosphate buffer (pH 6.5). Assays contained 25 μM 2,4-dinitrophenyl β-D-glucopyranoside as substrate and 1 mg/mL bovine serum albumin in a total volume of 1 mL. Reactions were initiated by addition of 10 μL of *Ss*GH1 to a final concentration of 2.2 nM, which was at least 10 times lower than the inhibitor concentration used. 2,4-Dinitrophenolate release was monitored continuously at 400 nm for a 600 s period. K_i values were determined by monitoring the rates directly in the presence (v_i) (between 25 and 200 nM for **1** and 20 nM for **2**) and absence (v_0) of inhibitor. Rates were taken as the slope of the line between 200 and 300 s or in the linear region following slow onset inhibition. The fractional decrease in v_0/v_i for each inhibitor was calculated using the equation $v_0/v_i = 1 + [I]/K_i$, and the mean K_i value was taken.

RESULTS

It is widely assumed that family GH1 enzymes acting on gluco-configured substrates harness a $^4H_3$ or ^4E transition state conformation, which is mimicked by compounds **1** and **2**. Kinetic data indeed show that **1** and **2** inhibit *Tm*GH1 and *Ss*GH1 extremely potently; at the pH optimum for inhibition with *Tm*GH1, **1** and **2** display K_i values of 74 and 2.8 nM, respectively. K_i values at the pH optimum of *Tm*GH1 catalytic activity (pH 5.8) are 138 and 7.5 nM for **1** and **2**, respectively, and at the optimum of *Ss*GH1 activity (pH 6.5) are 53 and ≤0.6 nM, respectively.

The pH profile of k_{cat}/K_M for *Tm*GH1 is bell-shaped with a pH optimum between 5.8 and 6.0 (Figure 2); fitting to a bell-shaped ionization curve gives acidic and basic limb pK_a values of 5.3 and 7.0, respectively. The pH dependence of $1/K_i$ for **1** and **2** are similarly bell-shaped, with slight alkaline shifts relative to catalysis. The pH optimum for inhibition

Table 1: Data Processing and Refinement Statistics for *Tm*GH1 and *Ss*GH1 in Complex with **1** and **2**

	*Tm*GH1 with **1**	*Tm*GH1 with **2**	*Ss*GH1 with **1**	*Ss*GH1 with **2**
data collection beamline (ESRF)	ID14-4	ID14-1	ID14-1	BM14
resolution (outer shell) (Å)	30−2.15 (2.23−2.15)	30−1.97 (2.04−1.97)	40−2.15 (2.23−2.15)	30−2.30 (2.38−2.30)
space group	$P2_12_12_1$	$P2_12_12_1$	$P3_121$	$P3_121$
unit cell parameters	$a = 94.5$ Å	$a = 94.4$ Å	$a = b = 167.9$ Å	$a = b = 167.9$ Å
	$b = 94.9$ Å	$b = 94.5$ Å	$c = 93.4$ Å	$c = 95.9$ Å
	$c = 113.9$ Å	$c = 113.6$ Å	$\alpha = \beta = 90°$	$\alpha = \beta = 90°$
	$\alpha = \beta = \gamma = 90°$	$\alpha = \beta = \gamma = 90°$	$\gamma = 120°$	$\gamma = 120°$
R_{merge} (outer shell)	0.055 (0.445)	0.051 (0.394)	0.104 (0.400)	0.113 (0.449)
mean $I/\sigma I$ (outer shell)	29.0 (3.2)	21.9 (2.8)	12.5 (3.9)	11.5 (3.5)
completeness (outer shell) (%)	99.6 (98.2)	97.6 (97.9)	99.9 (100.0)	98.3 (93.9)
multiplicity (outer shell)	5.4 (4.3)	4.8 (3.5)	5.3 (5.1)	6.1 (5.7)
no. of unique reflections	55897	70563	83599	68632
R_{cryst}	0.192	0.192	0.176	0.191
R_{free}	0.247	0.244	0.215	0.246
rmsd for bonds (Å)	0.015	0.013	0.013	0.013
rmsd for angles (deg)	1.480	1.374	1.35	1.39
rmsd for chiral volume (Å^3)	0.107	0.094	0.097	0.098
no. of protein atoms	7338	7322	8197	8187
no. of ligand atoms	28	44	28	58
no. of water atoms	475	577	880	745
no. of other atoms	9	5	20	12
average main chain *B*-factor (Å^2)	41.3	31.7	34.7	41.6
average side chain *B*-factor (Å^2)	41.7	32.4	35.5	41.9
average ligand *B*-factor (Å^2)	35.6	31.4	26.6	36.2
average water *B*-factor (Å^2)	45.7	39.7	44.5	44.7
PDB entry	2CES	2CET	2CEQ	2CER

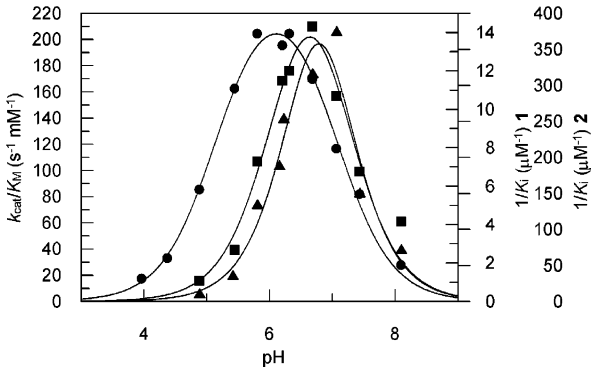

FIGURE 2: pH dependence of k_{cat}/K_M for *Tm*GH1 (●), $1/K_i$ for **1** (■), and $1/K_i$ for **2** (▲). Fits to bell-shaped ionization profiles are shown.

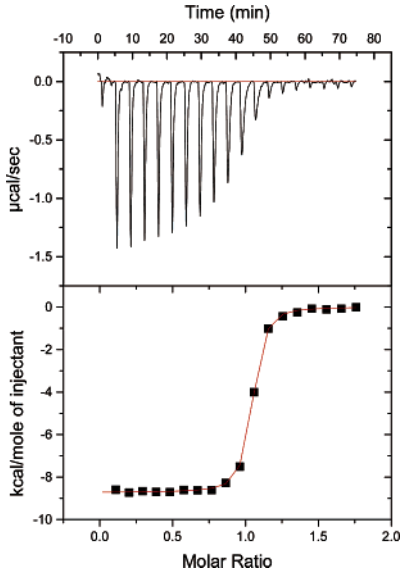

FIGURE 3: ITC data for binding of **1** to *Tm*GH1. The top panel shows the raw titration data of the power supplied to the system to maintain a constant temperature against time; the area of the peak gives the heat of interaction for each injection. The bottom panel shows the bimolecular fit of the normalized heats of interaction plotted against the molar concentration.

by **1** is around pH 6.6, with acidic and basic limb pK_a values of 6.2 and 7.1, respectively. The simplest explanation of the pH profiles is that the acidic limb is likely to reflect protonation of the inhibitor [which has a solution pK_a of 6.12 (*8*)] and the basic limb protonation of the acid/base residue. This suggests that at the pH optimum for *Tm*GH1 activity, **1** is bound in a predominantly protonated form, as experimentally observed with the cellobiose-derived form of **1** in complex with a family 5 endoglucanase using atomic resolution X-ray data (*23*). The pH optimum for inhibition by **2** is around pH 6.8, with acidic and basic limb pK_a values of 6.7 and 6.9, respectively. The titration profile for compound **2** is more difficult to interpret; the basic limb is likely to reflect protonation of the acid/base residue, but the acidic limb is not likely to reflect protonation of the nucleophile or the inhibitor [**2** has a solution pK_a of 6.03 (*9*)]. Such pH profile titrations are composites of events surrounding the enzyme, inhibitor, and enzyme−inhibitor complex and are notoriously difficult to interpret (*24*). It is likely that both inhibitors bind to *Tm*GH1 with one protonated and one deprotonated catalytic residue, in contrast to compounds such as isofagomine which bind most tightly to an inactive enzyme at high pH (*2*).

Similar binding constants for **1** and **2** are also derived from isothermal titration calorimetry (Figure 3), confirming that at the pH optimum for catalysis the glucoimidazole-derived compounds are indeed highly potent inhibitors of *Tm*GH1. Compounds **1** and **2** display K_d values of 56 and 9.6 nM, respectively, which agree extremely well with the K_i values derived kinetically (Table 2). Binding of **1** is shown to be driven by a large, favorable, enthalpic contribution, accompanied by a small, and also favorable, entropic contribution. Significantly, binding of **2** involves a much smaller (but

Table 2: Binding Constants for **1** and **2** with *Tm*GH1 Derived Using Kinetic and Thermodynamic Methods at pH 5.8, and the Thermodynamic Parameters Measured or Calculated Using ITC

	1	**2**
K_i (nM) (kinetics)	138	7.5
K_d (nM) (ITC)	56 ± 12	9.6 ± 0.5
$\Delta H_a°$ (kcal/mol)	−8.96 ± 0.24	−4.64 ± 0.32
$\Delta G_a°$ (kcal/mol)	−9.90	−10.93
$T\Delta S_a°$ (kcal/mol)	0.94	6.29

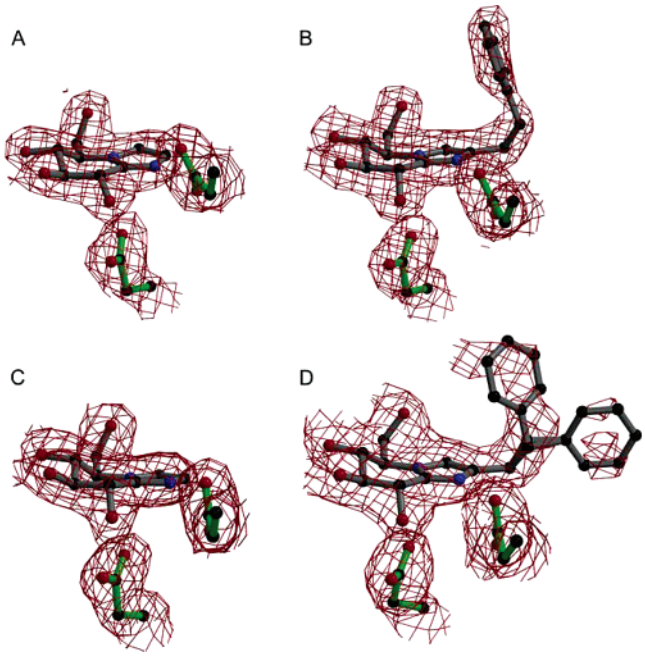

FIGURE 4: Ball-and-stick representation of (A) *Tm*GH1 [the nucleophile Glu351 (bottom) and acid/base Glu166 (right) are shown] bound to **1**, (B) *Tm*GH1 bound to **2**, (C) *Ss*GH1 [the nucleophile Glu387 (bottom) and acid/base Glu206 (right) are shown] bound to **1**, and (D) *Ss*GH1 bound to **2**. Observed electron density for the maximum likelihood weighted $2F_{obs} - F_{calc}$ map is contoured at 1σ in all cases. The figures were drawn using BOBSCRIPT (*29*) and rendered using RASTER3D (*30*).

still beneficial) enthalpy of interaction, but this is more than compensated by a considerably greater entropic contribution to binding. The effect from any protonation event that may occur upon ligand binding is not likely to contribute greatly to the enthalpy values as the heat of ionization of the sodium citrate buffer is extremely small (*21*).

It was widely assumed that **2**, which is substituted with a phenethyl group, would increase potency by virtue of productive interactions made with residues in the +1 subsite of the enzyme (*9*). The counterintuitive thermodynamic signatures of binding observed led us to study the structures of **1** and **2** in complex with *Tm*GH1, which was achieved with X-ray data to 2.15 and 1.97 Å resolution, respectively (Figure 4A,B). The interactions between *Tm*GH1 and **1** and **2** are essentially identical in both complexes (Figure 5A,B). The "glycoside" ring of **1** and **2** lies in an envelope (^4E) conformation. The hydroxyl group at C6 hydrogen bonds with the Oϵ2 atom of Glu405. The hydroxyl group at the C4 position interacts with the Oϵ1 atom of Glu405 and the amine group of Gln20, and the hydroxyl group at C3 hydrogen bonds with the carbonyl oxygen of Gln20, His121, and Trp406. The hydroxyl group at the C2 position interacts with the amine group of Asn165 and both atoms of the nucleophile, Glu351. The N2 atom of the imidazole moiety hydrogen bonds with both atoms of the lateral "anti-protonating" catalytic acid/base residue, Glu166, and with a water molecule (when in complex with **1** only). Superposition of the *Tm*GH1 complexes with **1** and **2** and the native structure shows there is movement of the acid/base residue, Glu166, about both the Cβ−Cγ and Cγ−Cδ bonds, to accommodate the imidazole moiety and to allow interactions with the nitrogen atom. Tyr295 also rotates away from the inhibitor binding site when in complex with **1**, presumably to prevent any unfavorable interactions with the imidazole group. Superposition of **1** and **2** indicates that the C2, C3, C4, and C5 substituents lie in the same position, but the imidazole moiety is tilted ~0.7 Å upward in the complex with **2**, meaning no movement of Tyr295 is required for accommodation of the ligand. Stunningly, however, the phenethyl group of **2** appears to make no interactions with active site residues in the +1 subsite as proposed by Panday and colleagues (*9*); instead, the phenethyl group points "upward". Despite making no productive interactions with the enzyme, the aglycon mimics the pseudoaxial conformation for the leaving group as observed on a number of glycosidase structures (*25*−*27*).

The surprising lack of interactions between **2** and *Tm*GH1, despite the extremely high potency, led to further structural investigation of both glucoimidazole compounds bound to a related family 1 glycosidase, *Ss*GH1. Data were collected to 2.15 and 2.30 Å resolution for complexes with **1** and **2**, respectively (Figure 4C,D). Once again, both compounds **1** and **2** are seen to adopt a ^4E conformation, and the interactions made between both compounds and the active site residues are essentially identical (Figure 5C,D). The hydroxyl group at C6 hydrogen bonds with the Oϵ2 atom of Glu432. The hydroxyl group at the C4 position interacts with the Oϵ1 atom of Glu432 and the amine group of Gln18. The carbonyl group of Gln18, the nitrogen atom of Trp433, and His150 hydrogen bond with the hydroxyl group at C3. The hydroxyl group at C2 interacts with the nitrogen atom of Asn205 and both oxygen atoms of the nucleophile, Glu387. Once again, the N2 atom in the imidazole ring makes cooperative hydrogen bond interactions with both oxygen atoms of the acid/base residue (Glu206) at distances of 2.6 and 2.9 Å. As observed for the *Tm*GH1 complex with **2**, no interactions between the phenethyl group of **2** and the active site residues exist. In complex with *Ss*GH1, however, the phenyl ring and the adjoining methylene group of **2** are present in two conformations. The electron density for this part of **2** is rather disordered, reflecting the mobility in this region. The two conformations of the phenyl ring coincide with a water molecule, which is also present in two positions; in one position, the water molecule hydrogen bonds with Glu432, whereas in the other position, it moves further toward **2** but appears to make no interactions.

DISCUSSION

1 and **2** have been shown to be highly potent inhibitors of β-glycosidases and are indeed among the most potent inhibitors studied to date for this class of enzyme. It is therefore pertinent to dissect in detail the binding profile for these glucoimidazole compounds, and to rationalize the features that make good inhibitors, which can be used to

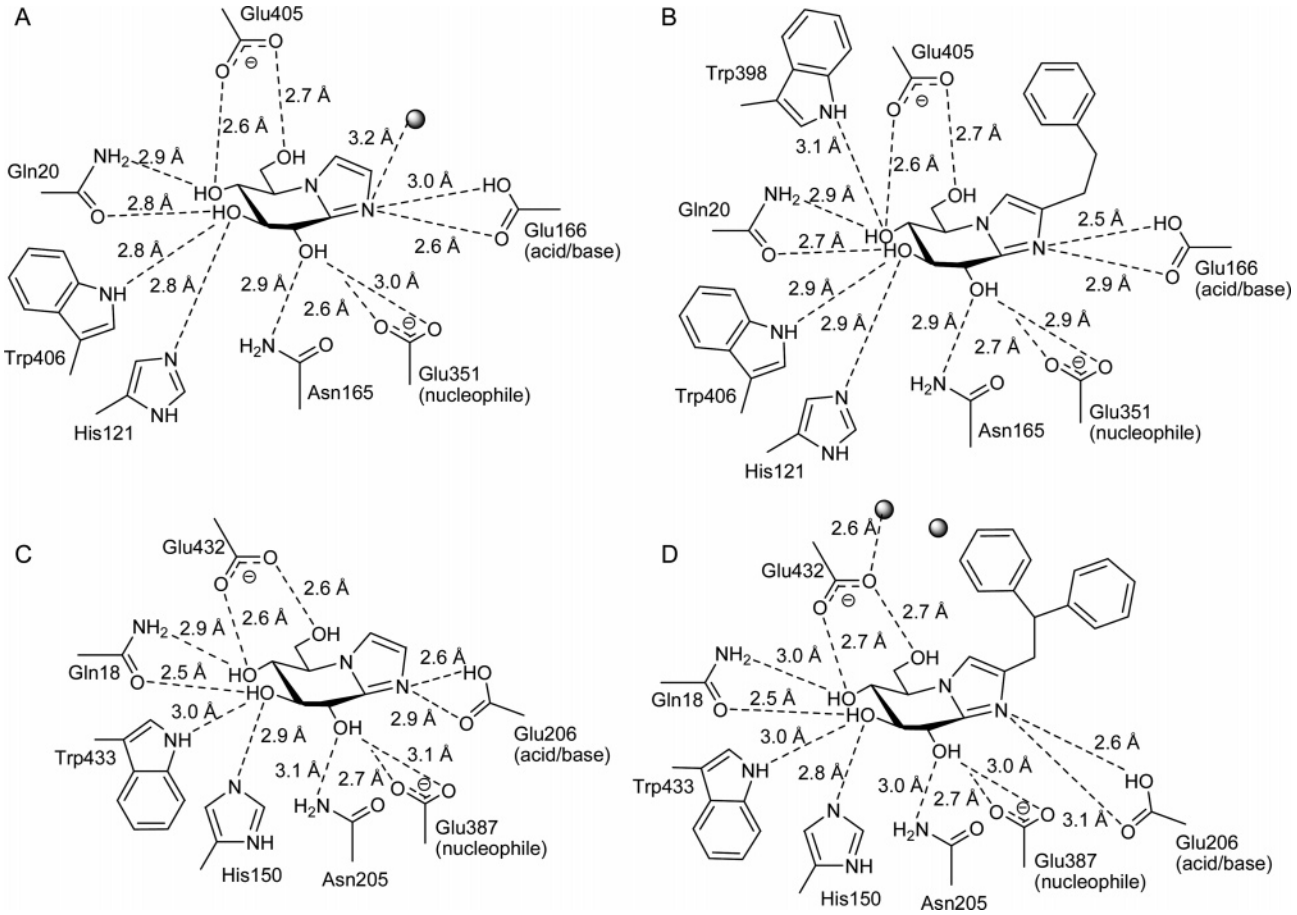

FIGURE 5: Interactions of *Tm*GH1 with (A) **1** and (B) **2** and *Ss*GH1 with (C) **1** and (D) **2**. The gray spheres represent water molecules.

drive the design of inhibitors in the future. Thermodynamic studies with compounds **1** and **2** have shown that the tighter binding of **2**, relative to that of **1**, appears to be driven by entropic forces. This, however, is at odds with Wolfenden's suggestion that the binding of true transition state mimics should be driven by enthalpy (*3*). Is **2** a weaker transition state mimic than **1**? In both *Tm*GH1 and *Ss*GH1, the phenethyl moiety of **2** makes no productive contacts with the enzyme and, in fact, appears to be disordered in particular in the complex with *Ss*GH1. These binding modes are in marked contrast to recent observations of binding of other glucoimidazoles possessing aromatic groups with a family GH3 β-D-glucohydrolase (*12*, *13*), where interactions between the aromatic group and an enzyme-derived tryptophan in the +1 subsite exist. It is significant, however, that the tighter binding of **2** than **1** is roughly equivalent on the three different systems, irrespective of the interactions made by the substituent groups. One contribution to the large entropy term for **2** may be the binding or release of water molecules from the protein (estimated from the crystal structures to be on the order of three to six water molecules), as has also been discussed for other glycosidase inhibitors with unusual thermodynamic signatures (*2*, *28*). However, one cannot investigate other thermodynamic terms such as the solvation of these compounds in free solution or their desolvation upon binding, which are very likely extremely significant thermodynamic contributors. The issues of solvent binding and release contributing in a significant fashion to glycosidase inhibition raise many questions for the future. The clear implication from this and other (*2*, *28*) work is that the forces governing binding are complex and that the thermodynamics of binding may not always correlate with expectation. It will, however, be important to test hypotheses on a wider spectrum of glycosidase inhibitors in the future. Although such work could have a potentially enormous impact on the design of inhibitors in the quest for highly potent and specific therapeutic agents, it is less clear how one optimizes inhibitors to influence complex binding terms such as solvation and desolvation.

ACKNOWLEDGMENT

The IBP-CNR belongs to the Centro Regionale di Competenza in Applicazioni Tecnologico-Industriali di Biomolecole e Biosistemi.

REFERENCES

1. Wolfenden, R., Lu, X., and Young, G. (1998) Spontaneous hydrolysis of glycosides, *J. Am. Chem. Soc. 120*, 6814−6815.
2. Zechel, D. L., Boraston, A. B., Gloster, T., Boraston, C. M., Macdonald, J. M., Tilbrook, D. M. G., Stick, R. V., and Davies, G. J. (2003) Iminosugar glycosidase inhibitors: Structural and thermodynamic dissection of the binding of isofagomine and 1-deoxynojirimycin to β-glucosidases, *J. Am. Chem. Soc. 125*, 14313−14323.
3. Wolfenden, R., Snider, M., Ridgway, C., and Miller, B. (1999) The temperature dependence of enzyme rate enhancements, *J. Am. Chem. Soc. 121*, 7419−7420.
4. Mader, M. M., and Bartlett, P. A. (1997) Binding energy and catalysis: The implications for transition-state analogs and catalytic antibodies, *Chem. Rev. 97*, 1281−1301.
5. Coutinho, P. M., and Henrissat, B. (1999) Carbohydrate-active enzymes: An integrated database approach, in *Recent advances in carbohydrate bioengineering* (Gilbert, H. J., Davies, G. J.,

Henrissat, B., and Svensson, B., Eds.) pp 3−12, Royal Society of Chemistry, Cambridge, U.K.
6. Davies, G. J., Ducros, V. M.-A., Varrot, A., and Zechel, D. L. (2003) Mapping the conformational itinerary of β-glycosidases by X-ray crystallography, *Biochem. Soc. Trans. 31*, 523−527.
7. Granier, T., Panday, N., and Vasella, A. (1997) Structure−activity relations for imidazo-pyridine-type inhibitors of β-D-glucosidases, *Helv. Chim. Acta 80*, 979−987.
8. Panday, N., and Vasella, A. (1999) Synthesis of glucose- and mannose-derived *N*-acetylamino imidazopyridines and their evaluation as inhibitors of glycosidases, *Synthesis*, 1459−1468.
9. Panday, N., Canac, Y., and Vasella, A. (2000) Very strong inhibition of glucosidases by *C(2)*-substituted tetrahydroimidazopyridines, *Helv. Chim. Acta 83*, 58−79.
10. Heightman, T. D., and Vasella, A. T. (1999) Recent insights into inhibition, structure, and mechanism of configuration-retaining glycosidases, *Angew. Chem., Int. Ed. 38*, 750−770.
11. Vasella, A., Davies, G. J., and Böhm, M. (2002) Glycosidase mechanisms, *Curr. Opin. Chem. Biol. 6*, 619−629.
12. Hrmova, M., de Gori, R., Smith, B. J., Vasella, A., Vargese, J. N., and Fincher, G. B. (2004) Three-dimensional structure of the barley β-D-glucan glucohydrolase in complex with a transition state mimic, *J. Biol. Chem. 279*, 4970−4980.
13. Hrmova, M., Streltsov, V. A., Smith, B. J., Vasella, A., Vargese, J. N., and Fincher, G. B. (2005) Structural rationale for low-nanomolar binding of transition state mimics to a family GH3 β-D-glucan glucohydrolase from barley, *Biochemistry 44*, 16529−16539.
14. Moracci, M., Ciaramella, M., and Rossi, M. (2001) β-Glycosidase from *Sulfolobus solfataricus*, *Methods Enzymol. 330*, 201−215.
15. Otwinowski, Z., and Minor, W. (1997) Processing of X-ray diffraction data collected in oscillation mode, *Methods Enzymol. 276*, 307−326.
16. Collaborative Computational Project Number 4 (1994) The *CCP*4 suite: programs for protein crystallography, *Acta Crystallogr. D50*, 760−763.
17. Murshudov, G. N., Vagin, A. A., and Dodson, E. J. (1997) Refinement of macromolecular structures by the maximum-likelihood method, *Acta Crystallogr. D53*, 240−255.
18. Navaza, J. (1994) *AMoRe*: An automated package for molecular replacement, *Acta Crystallogr. A50*, 157−163.
19. Brünger, A. T. (1992) Free *R* value: A novel statistical quantity for assessing the accuracy of crystal structures, *Nature 355*, 472−475.
20. Emsley, P., and Cowtan, K. (2004) Coot: Model-building tools for molecular graphics, *Acta Crystallogr. D60*, 2126−2132.
21. Goldberg, R. N., Kishore, N., and Lennen, R. M. (2002) Thermodynamic quantities for the ionization reactions of buffers, *J. Phys. Chem. Ref. Data 31*, 231−370.
22. Gloster, T. M., Madsen, R., and Davies, G. J. (2006) Dissection of conformationally restricted inhibitors binding to a β-glucosidase, *ChemBioChem 7*, 738−742.
23. Varrot, A., Schülein, M., Pipelier, M., Vasella, A., and Davies, G. J. (1999) Lateral protonation of a glycosidase inhibitor. Structure of the *Bacillus agaradhaerens* Cel5A in complex with a cellobiose-derived imidazole at 0.97 Å resolution, *J. Am. Chem. Soc. 121*, 2621−2622.
24. Knowles, J. R. (1976) The intrinsic pK_a-values of functional groups in enzymes: Improper deductions from the pH-dependence of steady-state parameters, *Crit. Rev. Biochem. 4*, 165−173.
25. Ducros, V., Zechel, D. L., Murshudov, G. N., Gilbert, H. J., Szabo, L., Stoll, D., Withers, S. G., and Davies, G. J. (2002) Substrate distortion by a β-mannanase: Snapshots of the Michaelis and covalent intermediate complexes suggest a $B_{2,5}$ conformation for the transition-state, *Angew. Chem., Int. Ed. 41*, 2824−2827.
26. Davies, G. J., Mackenzie, L., Varrot, A., Dauter, M., Brzozowski, A. M., Schulein, M., and Withers, S. G. (1998) Snapshots along an enzymatic reaction coordinate: Analysis of a retaining β-glycoside hydrolase, *Biochemistry 37*, 11707−11713.
27. Sulzenbacher, G., Driguez, H., Henrissat, B., Schulein, M., and Davies, G. J. (1996) Structure of the *Fusarium oxysporum* endoglucanase I with a nonhydrolyzable substrate analogue: Substrate distortion gives rise to the preferred axial orientation for the leaving group, *Biochemistry 35*, 15280−15287.
28. Gloster, T. M., Macdonald, J. M., Tarling, C. A., Stick, R. V., Withers, S. G., and Davies, G. J. (2004) Structural, thermodynamic and kinetic analyses of tetrahydrooxazine-derived inhibitors bound to β-glucosidases, *J. Biol. Chem. 279*, 49236−49242.
29. Esnouf, R. M. (1997) An extensively modified version of MolScript that includes greatly enhanced coloring capabilities, *J. Mol. Graphics Modell. 15*, 132−134.
30. Merritt, E. A., and Murphy, M. E. P. (1994) *Raster3D* version 2.0. A program for photorealistic molecular graphics, *Acta Crystallogr. D50*, 869−873.

BI060973X